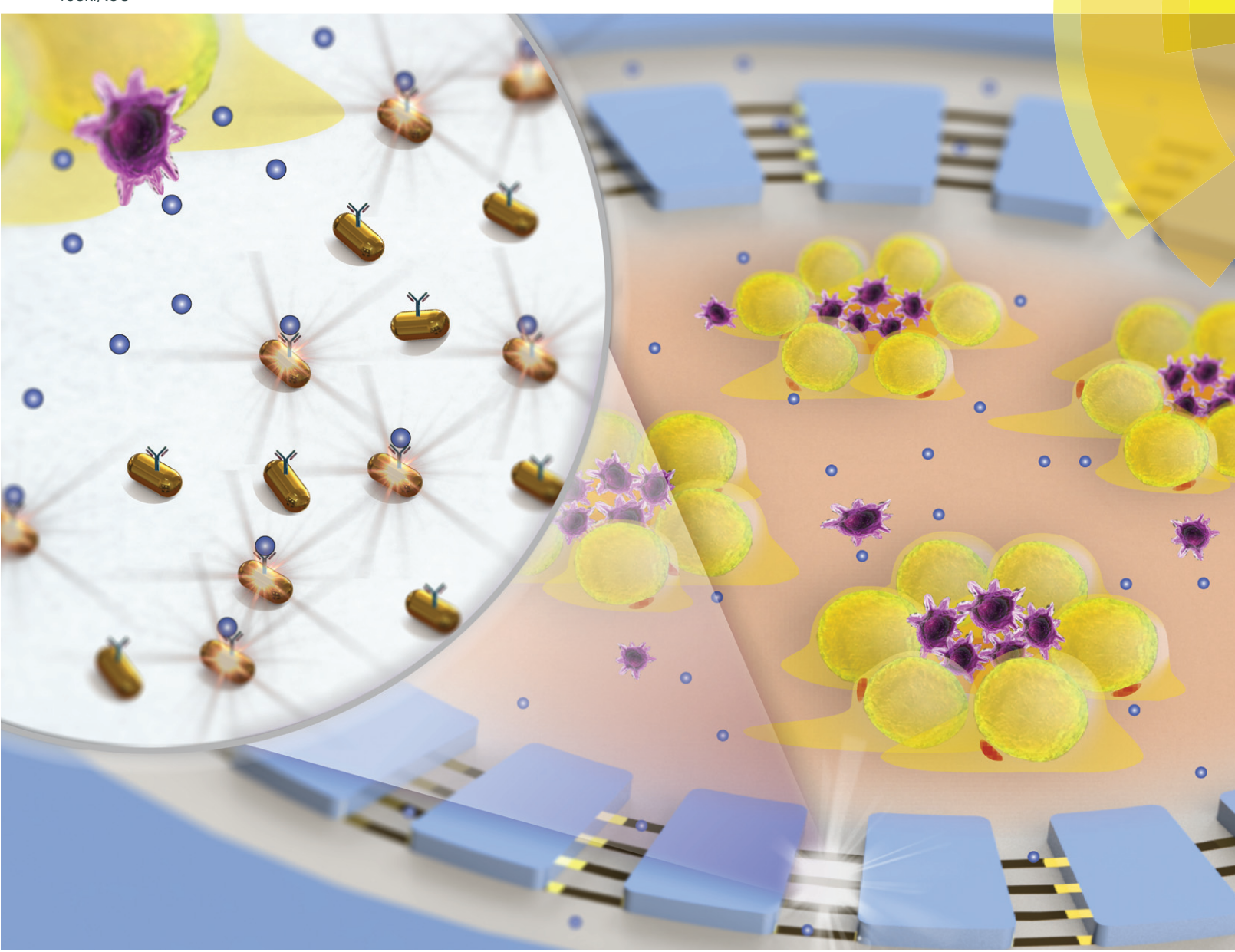
# LabonaChip

Devices and applications at the micro- and nanoscale rsc.li/loc



ISSN 1473-0197



## Lab on a Chip



PAPER View Article Online
View Journal | View Issue



Cite this: Lab Chip, 2018, 18, 3550

# An integrated adipose-tissue-on-chip nanoplasmonic biosensing platform for investigating obesity-associated inflammation†

Jingyi Zhu,<sup>a</sup> Jiacheng He,<sup>b</sup> Michael Verano,<sup>c</sup> Ayoola T. Brimmo,<sup>ad</sup> Ayoub Glia,<sup>ad</sup> Mohammad A. Qasaimeh, <sup>Dad</sup> Pengyu Chen, <sup>Db</sup> Jose O. Aleman<sup>c</sup> and Weigiang Chen <sup>D\*ae</sup>

Although many advanced biosensing techniques have been proposed for cytokine profiling, there are no clinically available methods that integrate high-resolution immune cell monitoring and *in situ* multiplexed cytokine detection together in a biomimetic tissue microenvironment. The primary challenge arises due to the lack of suitable label-free sensing techniques and difficulty for sensor integration. In this work, we demonstrated a novel integration of a localized-surface plasmon resonance (LSPR)-based biosensor with a biomimetic microfluidic 'adipose-tissue-on-chip' platform for an *in situ* label-free, high-throughput and multiplexed cytokine secretion analysis of obese adipose tissue. Using our established adipose-tissue-on-chip platform, we were able to monitor the adipose tissue initiation, differentiation, and maturation and simulate the hallmark formation of crown-like structures (CLSs) during pro-inflammatory stimulation. With integrated antibody-conjugated LSPR barcode sensor arrays, our platform enables simultaneous multiplexed measurements of pro-inflammatory (IL-6 and TNF- $\alpha$ ) and anti-inflammatory (IL-10 and IL-4) cytokines secreted by the adipocytes and macrophages. As a result, our adipose-tissue-on-chip platform is capable of identifying stage-specific cytokine secretion profiles from a complex milieu during obesity progression, highlighting its potential as a high-throughput preclinical readout for personalized obesity treatment strategies.

Received 14th June 2018, Accepted 29th September 2018

DOI: 10.1039/c8lc00605a

rsc.li/loc

#### Introduction

The adipose tissue of obese patients is characterized as a tissue microenvironment composed of adipose tissue macrophages, precursor and hypertrophic adipocytes, and other immune cells that predominantly produce pro-inflammatory cytokines, such as IL-6, IL-1 $\beta$ , and TNF- $\alpha$ , for chronic, low-grade inflammation. Adipose tissue inflammation is a critical risk factor of obesity and is linked to the development of complications like type 2 diabetes mellitus, cardiovascular diseases and certain cancers. Pathologically, inflammation in

obese adipose tissue has been defined as the accumulation of

immune cells, specifically macrophages, around a necrotizing adipocyte, an entity known as a crown-like structure (CLS).<sup>3,4</sup>

There is a limited understanding of obesity-associated inflam-

mation in an adipose tissue microenvironment during disease

Cytokines are key immune regulators of inflammation and form complex immune-body cytokine networks for intercellular communications among immune cells and parenchymal cells of organs and tissues.<sup>7</sup> Precisely quantifying cytokine secretions from immune and body cells remains a critical challenge due to their small molecule size, extremely low concentrations, and transient alterations during cell-cell signaling in the extracellular milieu.<sup>8,9</sup> The enzyme-linked immunosorbent assay (ELISA) is widely used and regarded as

progression. Previous studies of adipose tissue inflammation have mostly focused on *ex vivo* studies of CLS using adipose tissues isolated from mouse models or patient surgical waste, <sup>3,4</sup> or characterizing the immunogenicity of adipocyte cell lines without a local, chronic inflammatory milieu. <sup>5,6</sup> Hence, there is a demand for a platform that can report the spatiotemporal dynamics of cell cytokine secretion profiles during adipocyte differentiation and CLS formation and resolution in an adipose tissue microenvironment.

<sup>&</sup>lt;sup>a</sup> Department of Mechanical and Aerospace Engineering, New York University, New York, NY, USA. E-mail: wchen@nyu.edu

<sup>&</sup>lt;sup>b</sup> Materials Research and Education Center, Materials Engineering, Department of Mechanical Engineering, Auburn University, Auburn, AL, USA

<sup>&</sup>lt;sup>c</sup> Laboratory of Translational Obesity Research, Division of Endocrinology, Department of Medicine, New York University School of Medicine, New York, NY,

<sup>&</sup>lt;sup>d</sup> Division of Engineering, New York University Abu Dhabi, Abu Dhabi, United Arab Emirates

 $<sup>^</sup>e$ Department of Biomedical Engineering, New York University, New York, NY, USA  $\dagger$  Electronic supplementary information (ESI) available. See DOI: 10.1039/c8lc00605a

a "gold standard" method for cytokine profiling. Conventional ELISAs rely on fluorescence labeling, long-term sample incubation and time-consuming manipulation processes, which greatly limit the real-time, multiplexed cytokine measurements and the ability to monitor cell functions in a dynamic manner under niche-specific conditions. 10 Recently, a few label-free detection strategies such as mechanical, 11,12 electrochemical, 13-16 optical, 17-19 or surface plasmon resonancebased biosensors<sup>20-24</sup> have been developed for real-time profiling multiplexed cytokines in biological fluid samples, such as serum, 13 urine, or saliva. 13 However, tools to measure cytokine secretion dynamics and the associated cellular immune functions within immune-body tissue microenvironments remain in their infancy, owing to difficulties in measurement set-up for signal acquisition and sensor integration.

Recent advances in lab-on-a-chip technologies have allowed the integration of cytokine biosensors and made onchip cell culture possible.25 For example, Luchansky et al.26 and Oh et al.27 have demonstrated platforms capable of dynamic and multiplexed T-cell cytokine secretion profiling using integrated microfluidic devices with a silicon microring resonator sensor and nanoplasmonic gold nanoparticle sensor, respectively. However, these methodologies still cannot achieve on-chip, in situ measurements from cells due to laborious sample preparation steps of separating supernatants from cell culture. Others have shown microfluidic biosensing devices capable of on-chip immune cell isolation and integrated with nanoplasmonic<sup>28-30</sup> or AlphaLISA<sup>31,32</sup> sensors for detecting cytokine secretions of live cells. However, until now, there is still a lack of technologies that can achieve label-free, dynamic, and multiplexed cytokine profiling to monitor cellular functions in situ in a biomimetic tissue environment. Importantly, the need of sampling for these detection technologies will affect the original concentrations of cytokines released by the cells, compromising the ability to continuously monitor cell secretion profiles for extended culture periods (during cell differentiation and polarization). This limitation becomes even more pronounced when studying an on-chip bio-mimic system with small volume of medium contained in a microfluidic chip ( $<100 \mu L$ ).

In this work, we demonstrate, for the first time, a novel, integrated microfluidic 'adipose-tissue-on-chip' platform for in situ, high-throughput, multiplexed analysis of cytokine secretion dynamics within a biomimetic adipose tissue microenvironment. Our biomimetic 'adipose-tissue-on-chip' platform permits a real-time, chronological observation of the dynamic stages of adipocyte differentiation and CLS formation. Simultaneously, we equipped a label-free localized surface plasmon resonance (LSPR)-based nanoplasmonic biosensor 10,28,33,34 to the biomimetic adipose tissue microenvironment for in situ cytokine monitoring of adipose tissue inflammation. Multiplexed measurements of cytokine concentrations were achieved with a unique dark-field imaging scheme using antibody-conjugated gold nanorod (AuNR) LSPR nanobiosensor barcode microarrays.<sup>27,35</sup> This on-chip immunoassay technology affords a wide dynamic cytokine detection

range (~10-10 000 pg mL<sup>-1</sup>) and requires a low operating sample volume (down to ~1  $\mu$ L) and short assay time (~30 min). More importantly, our label-free, imaging-based LSPR immunoassay is ideal for an in situ, dynamic monitoring of proinflammatory [tumor necrosis factor alpha (TNF-α) and interleukin-6 (IL-6)] and anti-inflammatory [interleukin-10 (IL-10) and interleukin-4 (IL-4)] cytokine secretions from the adipose tissue inflammation. Our platform eliminates the need of sampling by avoiding complex culture medium separation procedures, which allows on-chip culture and continuous monitoring without perturbing cell/tissue microenvironments. Using our platform, we can quantitatively characterize a time-course functional response of adipocytes under inflammatory stimulation, as well as the immunophenotype switch of macrophages in an inflammatory adipose tissue microenvironment. This may facilitate the future development of new prognostic tools useful for personalized treatment strategies that address problems in obesity and its complications.

#### Results and discussion

#### Integrated adipose-tissue-on-chip nanoplasmonic biosensing platform design

The integrated 'adipose-tissue-on-chip' used in this study consists of two components: a central adipose tissue culture chamber and a peripheral nanoplasmonic LSPR sensing array (Fig. 1a and S1†). A polydimethylsiloxane (PDMS) layer with an incubation chamber (4 mm central diameter) was fabricated and bound to cover the glass for adipose-tissue-on-chip culture. It has been considered that the formation of CLS composed of dead adipocytes surrounded by macrophages is a defining hallmark of obesity and adipose tissue dysfunction.<sup>36</sup> Therefore, in this study, we presented a biomimetic culture model using murine adipocytes and macrophages, which are the predominant cells that are present in CLS and mediate inflammation in obese adipose tissue to form a biomimetic adipose tissue microenvironment. 3T3L1 cells, a widely-used precursor adipocyte line, and J774A.1 (J7) mouse macrophages were used and cultured in the central chamber at 37 °C and 5% CO<sub>2</sub> conditions for 15 days for the on-chip formation of CLSs of obese adipose tissue (Fig. 1b).

To achieve a complete profile of immune-cell cytokine secretion, we integrated a LSPR 'barcode' sensing array of four circular AuNR stripes aligned perpendicularly to the microchannel (1000 µm long, 200 µm wide) patterns surrounding the adipose tissue chamber for cytokine detection (Fig. S1†). Each LSPR AuNR detection stripe has a width of 100 μm and an inter-bar gap of 100 µm and functionalized with different cytokine detection antibodies on another glass layer using a one-step microfluidic patterning method (Fig. S1d and S2†). The assembled device allows cell culture medium to diffuse from the adipose tissue chamber into the microchannels and interact with the AuNR barcodes for the "label-free" cytokine detection of the adipose tissue microenvironment (Fig. 1b and S1c†). The integrated microfluidic adipose-tissue-on-chip coupled with LSPR dark-field imaging permitted us to

Paper Lab on a Chip

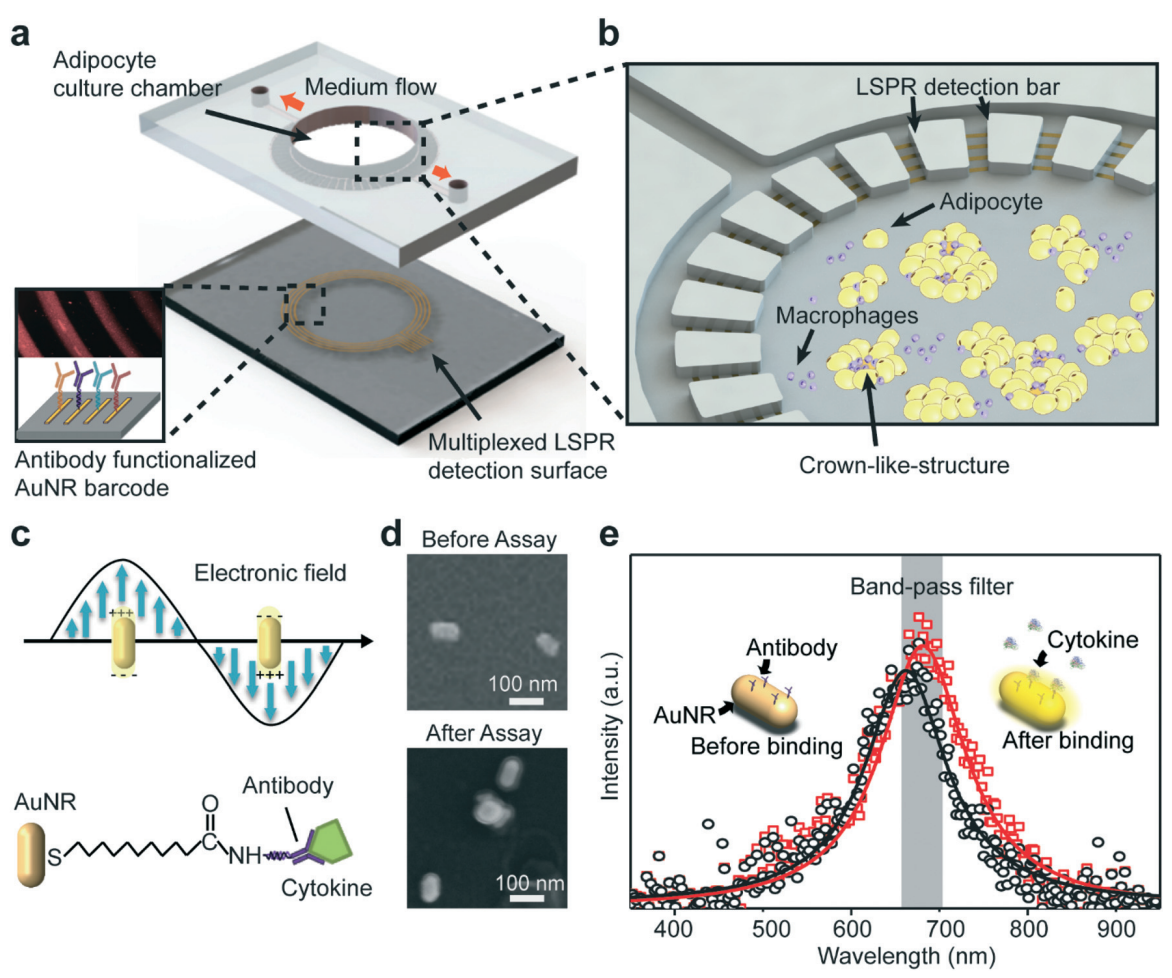


Fig. 1 Adipose-tissue-on-chip sensing platform for an *in situ* multiplexed analysis of adipose tissue inflammation. (a) Schematic of the integrated LSPR optofluidic platform device. The bottom layer is an AuNR-patterned barcode for multiplexed LSPR detection. The top PDMS layer provides a cell culturing chamber for adipocyte culturing and observation for on-chip CLS formation with introduction of macrophages. (b) Enlarged schematic shows that the adipocyte culture chamber is surrounded by multiple microchannels connected to LSPR cytokine detection barcode arrays. The circular LSPR sensing arrays are aligned and covered under the microchannel patterns surrounding the cell culturing chamber. The adipocyte and macrophage culture medium supernatant is then diffused into the microchannels and interacts with the AuNR LSPR sensors. (c) Principle of LSPR-based biosensing with cytokine-binding events on AuNRs. (d) SEM images of individual AuNR biosensors immobilized on glass before and after immunoassay. After the cytokine assay, the AuNR surfaces show a protein-coated layer. (e) Principle of dark-field intensity imaging of LSPR nanoplasmonic biosensor microarrays, where the binding between the targeted antigen and sensing surface induces spectral redshift and intrinsic intensity enhancement of AuNR scattering light. Measuring intensity changes with a band-pass filter enables us to quantify the analyte concentration in the samples.

conduct functional immunoassay for the *in situ*, multiplexed monitoring of a group of immune cells secreting cytokines from the adipose tissue microenvironment. Such a device can be readily used to provide predictive information and mechanistic insights for unraveling the complex, adaptive nature of obese adipose tissue in a proinflammatory milieu under macrophage recruitment.

## Cytokine detection standard curve acquisition and validation with ELISA

LSPR is a plasmonic phenomenon that arises from nanoscale structures or nanoparticles of a conductive metal (AuNRs in this study) when its surface is illuminated with light (Fig. 1c and d).<sup>37</sup> When the incident light frequency matches

the natural frequency of the electron oscillation of the AuNRs, it generates significantly enhanced near-field LSPR "hot spots" at the corners of the nanoparticles and results in an increased number of scattered photons in far-field, which are sensitive to the condition changes in the vicinity of metal nanoparticles. Cytokine binding events lead to changes in the near-field refractive index around AuNRs, shifting the intensity and phase of the extinction spectra (Fig. 1e) and, thus, increasing dark-field LSPR image brightness. Applying this LSPR mechanism, we established a microfluidic dark-field imaging platform for rapid, precise, and dynamic cytokine measurements (Fig. S3a†).

The layout and preparation of LSPR AuNR strips are shown in Fig. 1a and S2† (see details in Materials and methods). Aqueous cetrimonium bromide (CTAB)-coated

AuNRs (NanoSeedz Ltd.) with average lengths of 80 ± 5 nm and widths of 40  $\pm$  3 nm were used as the sensing elements and uniformly distributed on the glass substrate with an interparticle distance of >100 nm to avoid plasmonic coupling between adjacent particles (Fig. 1d). Before the detection, we first functionalized each of the four AuNR strips with cytokine-specific antibodies targeting pro-inflammatory (TNFα and IL-6) and anti-inflammatory (IL-10 and IL-4) cytokines using standard EDC/NHS chemistry (see details in Materials and methods, Fig. 1a, and S2†). After the cytokine binding, a ~10 nm thick protein layer coating on the AuNRs was observed, which further confirms the binding of antibody/cytokine molecules to the sensor surface. We also monitored the spectral red-shift at the end of each bio-conjugation step during the AuNR surface functionalization and after the measurement of 10 ng mL<sup>-1</sup> of IL-6 using a spectrophotometer attached to a microscope (Fig. S3b† and 1e). In our measurement, we observed that the resonance peak wavelength of the extinction spectrum of our AuNRs on the glass substrate was shifted from 662 nm to around 681 nm, confirming the cytokine binding events to the sensor surface.

The integrated nanoplasmonic biosensing platform was then mounted on a dark-field microscopy stage for rapid, high-sensitivity, and dynamic cytokine detection (Fig. 2a and

S3a;† see details in Materials and methods). The scattering spectrum can be spatially mapped across the surface to obtain a LSPR image. An increase in the surface antigen-antibody binding thus increases the brightness of the LSPR image. The LSPR images of the AuNR nanoplasmonic biosensor microarrays were captured in real time using a 10× objective lens, a dark-field condenser, an electron multiplying chargecoupled device (EMCCD) through a band-pass filter (674-686 nm) (Fig. 2a and Fig. S3a†). The captured LSPR images were then processed using a customized MATLAB program to selectively detect the intensity changes of the LSPR images in a microfluidic channel resulting from the cytokine surface binding to AuNRs (Fig. 1a).

Prior to multiplexed analyte detection, we performed parallel measurements of different cytokines using the LSPR sensing units on the microfluidic chip. Standard curves were acquired for each cytokine to determine the assay time, dynamic range and limit of detection (LOD) of the sensors. First, we measured real-time cytokine signal variations associated with analyte surface binding in a multiplexed scheme with a mixture of four target cytokines suspended in phosphate buffered saline (PBS) solution. In the cytokine solution, a different concentration level was assigned to cytokines IL-4, IL-6, IL-10 and TNF- $\alpha$ , at 3000, 1000, 500, and 250 pg mL<sup>-1</sup>,

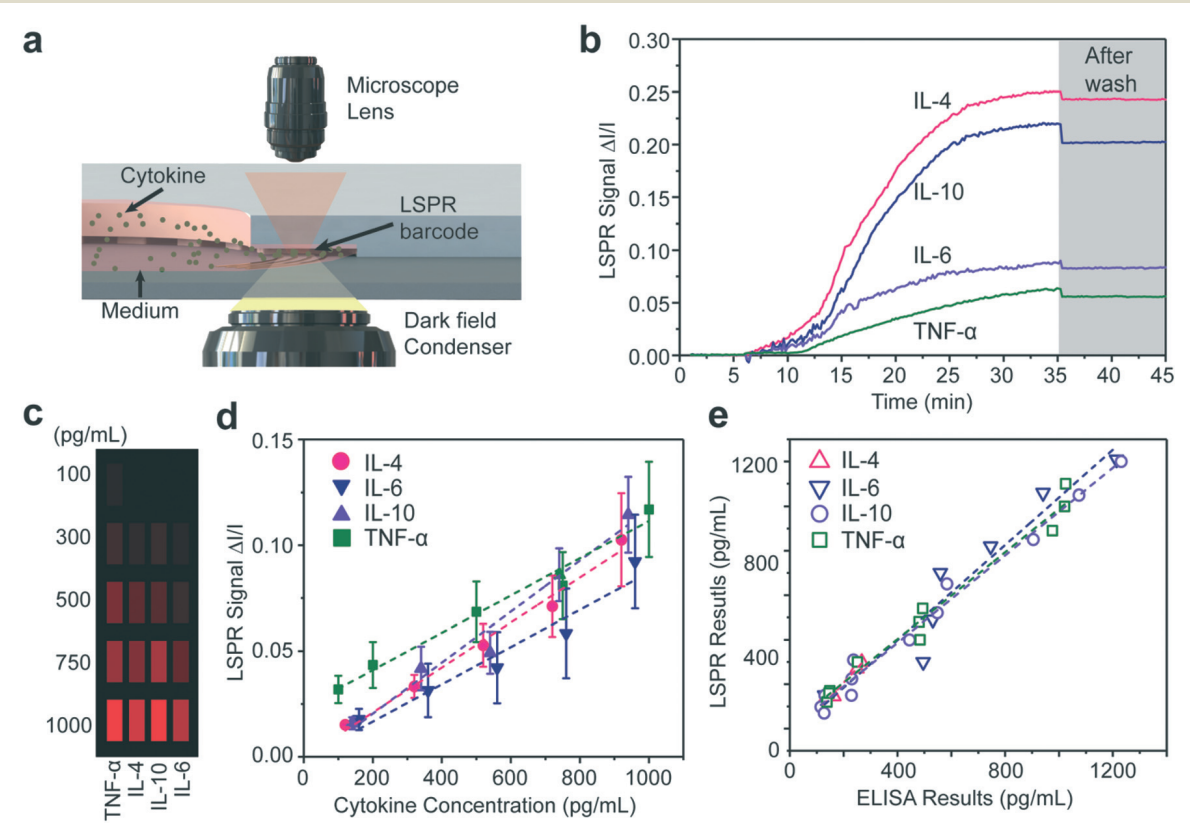


Fig. 2 Label-free and multiplexed nanoplasmonic measurement of cell-secreted cytokines. (a) Schematic of LSPR signal detection on a dark-field microscopy stage. (b) Real-time LSPR signals during the multiplexed cytokine detection. The gray area shows the LSPR signal after washing with PBS. (c) Mapping of intensity variations at LSPR microarray sensing spots for four different types of cytokines at different concentrations. (d) Calibration curves of purified IL-4, IL-6, IL-10, and TNF-α obtained from the LSPR nanoplasmonic biosensor microarray chip. Each sample was measured ten times. Error bar: standard error. (e) Correlation between data obtained from independent LSPR microarray and gold standard ELISA experiments using the same samples.

Paper Lab on a Chip

respectively. We loaded the cytokine mixture into one of the microfluidic channels of the LSPR microarray device and subsequently measured the time-course signal variation from the sensor spots (Fig. 2b). Analyte-antibody binding reached equilibrium within 30 min after the introduction of the cytokine mixture, as evidenced by signal plateaus. The rapid analyte binding kinetics allowed the assay to be performed with a very short incubation time, without adversely affecting the on-chip cell culture. Such a time-saving detection tool for multiplexed cytokine profiling can be performed at the point of interest during adipose tissue-on-a-chip culture. The signal intensity was only reduced by ~8% after washing with PBS to remove any nonspecific bound molecules. We then spiked a PBS solution with purified IL-4, IL-6, IL-10 and TNF- $\alpha$  with known concentrations from 100 to 1000 pg mL<sup>-1</sup> and quantified the percentage of scattering intensity change induced by the specific binding of target analyte cytokines to antibodyconjugated AuNR microarrays. Fig. 2c shows the mapping of intensity variations at our LSPR microarray sensing spots for the four different types of cytokines at varying concentrations. We recorded the intensity values of the LSPR sensing spots before (I) and after  $(I + \Delta I)$  sample incubation and plotted standard curves showing the fractional intensity shift  $\Delta I/I$ as a function of cytokine concentrations (Fig. 2d).

We further compared the readouts from the LSPR nanoplasmonic biosensor with those obtained using the "gold standard" ELISA (Biolegend) (Fig. 2e). The PBS solutions spiked with different concentrations of cytokines were tested using both the LSPR biosensors and ELISA. We found an excellent correlation between the two types of measurements across a wide dynamic range with slope values of 1.069, 0.982, 1.305, and 0.976 and  $R^2$  of 0.918, 0.985, 0.983, and 0.979 for cytokines IL-6, TNF-α, IL-4 and IL-10, correspondingly. Therefore, we validated the accuracy of our LSPR nanoplasmonic biosensors. It should be noted that typical ELISA measurements require at least 100 µL of sample medium for each cytokine detection. Thus, a total of at least 400 µL media is required to measure 4 types of cytokines. However, the in vitro adipose-tissue-on-chip in this study only requires a few microliters of samples, which is inaccessible by conventional ELISA.

#### On-chip adipose tissue cell culture

To form a biomimetic adipose tissue microenvironment, 3T3L1 precursor adipocyte cells and J7 mouse macrophages were used and cultured in the adipose tissue chamber for 15 days (Fig. 3a). We quantitatively characterized time-course responses of adipocytes during maturation and inflammatory stimulation and obtained a dynamic correlation between the cytokine secretion profile under adipocyte differentiation and CLS formation (Fig. 3b) within the adipose tissue microenvironment. Initially, 1000 3T3L1 pre-adipocytes were loaded into the culturing chamber (day 0) and treated with differentiation medium (see Materials and methods) for 2 days to initiate adipocyte differentiation. Following that, the adipocytes were continuously cultured in the maintenance medium for

another 11 days. Pioglitazone is recognized to activate PPAR alpha to differentiate pre-adipocytes into mature adipocytes. Thus, we accelerated the maturation of adipocytes in our in vitro system by adding 0.2 µM pioglitazone into the maintenance medium on day 2.5 As shown in Fig. 3c, the 3T3L1 cells treated with pioglitazone exhibited a unique adipocyte morphology, evidenced by increasing accumulation of lipid drops and many signet ring appearances of adipose cells.<sup>38</sup>

After day 13, 2 ng mL<sup>-1</sup> of purified TNF-α were added to the cell culture chamber to trigger the pro-inflammatory response from the adipocytes as well as to promote the necrosis of adipocytes, mimicking the dysfunctional adipose tissue with chronic inflammation caused by obesity. After a 24-hour incubation, the medium with TNF-α was removed and replaced by fresh maintenance medium on day 14. Subsequently, different densities of J7 macrophages (0, 500, and 1000 cells, denoted as 0× Mac, 1× Mac and 2× Mac in Fig. 4) were introduced into the three different devices to imitate different levels of macrophage infiltration, respectively. After fifteen days of adipocyte differentiation, maturation, and inflammatory stimulation, bio-mimic CLSs consisting of macrophages encircling a necrotizing adipocyte<sup>3,4</sup> were successfully observed in our microfluidic chip, validating adipose tissue inflammation in the adipose tissue microenvironment. Fig. 3b presents the fluorescence image of the adipocytes, macrophages, and CLS on the chip after cell fixing and staining on day 15. The macrophages were stained with an iNOS M1 macrophage marker (red color) and the nuclei of adipocyte were stained with DAPI (blue color). Clearly, there are a number of CLS signatures by clusters of macrophages circulating adipocytes. We confirmed that the macrophages in CLS are mostly polarized to the M1 pro-inflammatory phenotype.<sup>39</sup> This observation confirmed that we have successfully created an inflammatory adipose tissue. The polarization of macrophages also concurs with the results from in vivo observations from obese human and mice.36,40 Moreover, we can directly observe the CLS on-chip even without fluorescence staining, owing to the unique appearance of CLS (Fig. 3c). We observed that the density of CLS is positively correlated with an increasing number of J7 macrophages (Fig. S4†), indicating that the number of recruited macrophages may correlate with the level of inflammation in the adipose tissue.

#### On-chip cytokine secretion profile measurement from the adipocytes and adipose tissue macrophages

During the progression of obesity, the adipose tissue macrophages and hypertrophic adipocytes produce a proinflammatory milieu of cytokines, such as IL-6 and TNF- $\alpha$ , for facilitating chronic low-grade inflammation.<sup>1,2</sup> Therefore, in situ multiplexed cytokine profiling is a key to monitoring the status changes of adipose tissue inflammation from an initiation to a chronic stage, as indicated by the CLS formation. To obtain the multiplexed adipocyte cytokine secretion profile from the adipose tissue cells and macrophages, we

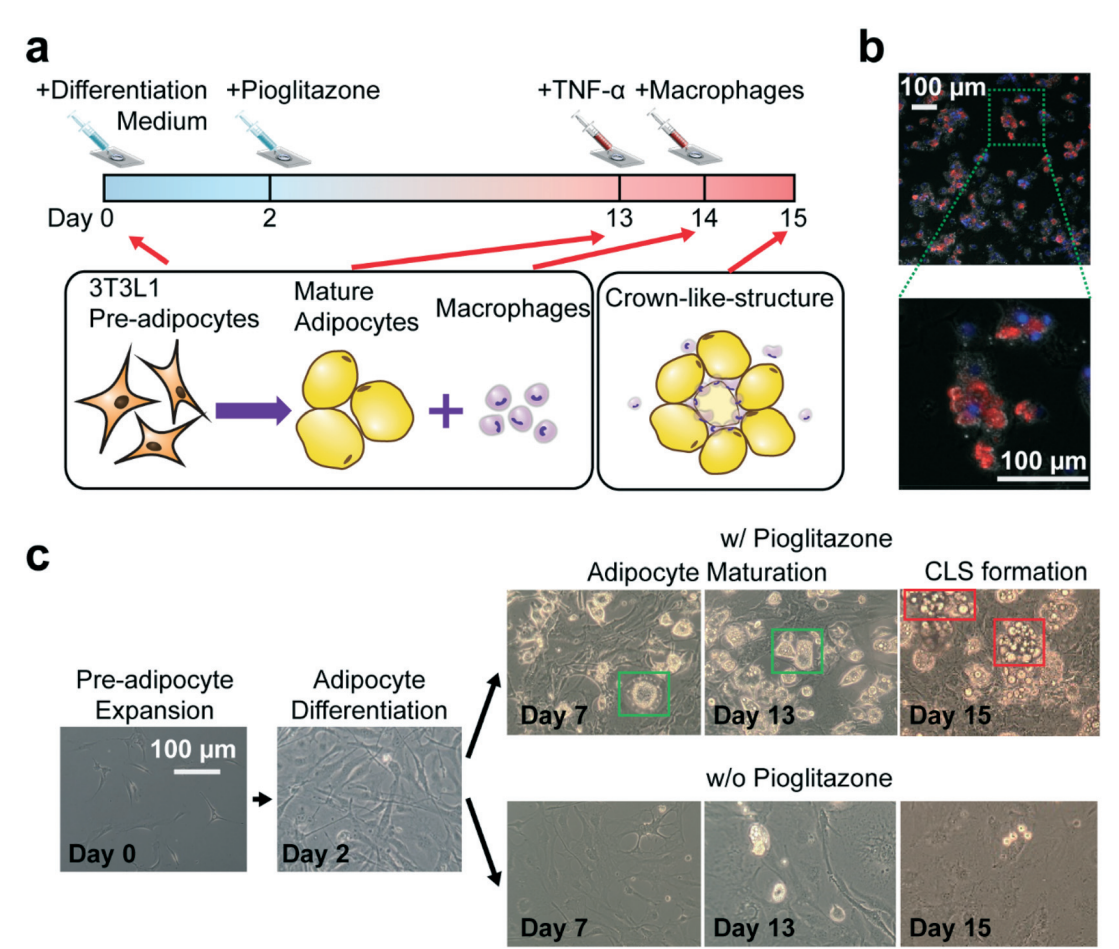


Fig. 3 On-chip adipocyte culture, differentiation, inflammatory stimulation, and CLS formation. (a) Schematic of the on-chip adipocyte culture, differentiation, inflammatory stimulation, and CLS formation process. After the 3T3L1 pre-adipocytes were loaded into the adipocyte culture chamber, the cell culture and expansion medium were replaced with the differentiation medium to initiate adipocyte differentiation, and we denoted the date as day 0. To enhance adipocyte differentiation, 0.2 µM pioglitazone was added into the maintenance medium on day 2. The adipocytes were then continuously cultured in the maintenance medium with pioglitazone for another 11 days. On day 13, 2 ng mL<sup>-1</sup> of TNF- $\alpha$  was added into the medium, stimulating the inflammatory microenvironment. The macrophages were added on day 14. Subsequently, the formation of CLSs was observed on day 15. (b) Representative fluorescence image of the adipocytes, macrophages, and CLS on the chip. The nucleus of adipocytes was stained using DAPI (blue color) and the macrophages were stained using an iNOS M1 macrophage marker (red color). The enlarged image clearly shows a CLS with M1 macrophages surrounding the adipocyte cells. (c) Optical microscopy images of the on-chip adipocyte differentiation and CLS formation process. The 3T3L1 cells treated with pioglitazone exhibited a unique mature adipocyte morphology, evidenced by increasing accumulation of lipid drops and many signet ring appearances of adipose cells.

prepared the LSPR sensing arrays on glass slides with each AuNR barcode functionalized by antibodies targeting IL-4, IL-6, IL-10, or TNF- $\alpha$ , respectively (Fig. 4a). After each cytokine measurement, we peeled off the glass slide deposited with AuNRs, and replenished the incubation chamber with a fresh cell culture medium. We quantitatively measured the four cytokine secretion levels in the adipose-tissue-on-chip on day 0 (expansion medium), day 2 (differentiation medium), day 7 and day 13 (maintenance medium + pioglitazone), day 14 (maintenance medium + TNF-α), and day 15 (maintenance medium ± pioglitazone + J7 macrophages). The results were plotted as a heat map 'barcode" visual, as shown in Fig. 4b. The heat map sensing barcode provides a multiparametric and spatiotemporal analysis of the immune status of the adipose tissue microenvironment. It is noteworthy that antiinflammatory cytokines, especially IL-4, were nearly

undetectable. However, pro-inflammatory cytokines were observed predominantly in concentrations on day 14 and day 15, confirming that a pro-inflammatory microenvironment was formed after TNF- $\alpha$  stimulation.

We first compared the adipocyte cytokine secretion profiles during the differentiation process (from day 0-13) to after TNF- $\alpha$  stimulation (day 14). The secretion of antiinflammatory cytokine, IL-10, was the most prominent in healthy developing 3T3-L1 adipocytes under low-density macrophage culture or pioglitazone conditions. In Fig. 4c, we observed elevated secretions of IL-10 but negligible levels of other secretory cytokines from day 0-13, confirming the healthy state of the adipocytes. Pioglitazone has previously been reported to suppress adipose tissue inflammation<sup>41</sup> and can be attributed to the observed increasing levels of antiinflammatory cytokine IL-10. On day 14 after 24 h of Paper Lab on a Chip

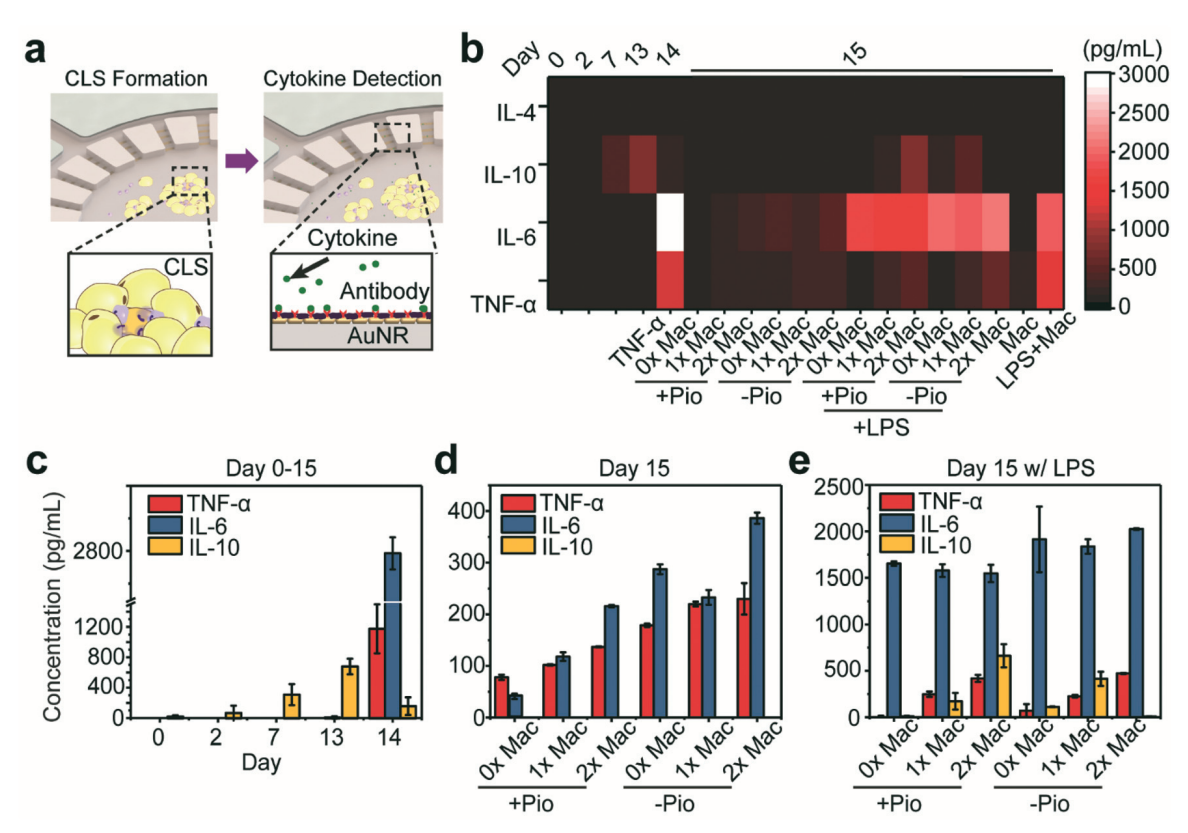


Fig. 4 On-chip multiplexed cytokine secretion profile measurement. (a) Schematic of on-chip CLS formation and cell-secreted cytokine detection. (b) A heat map visualization representing the concentrations of IL-4, IL-6, IL-10 and TNF- $\alpha$  at different stages of adipose-tissue-on-chip, with different concentration of macrophages and with/without different reagents such as Pio and LPS. (c) Cytokine secretion profiles of 3T3L1 adipocytes during the 13-day differentiation process. The adipocytes exhibited an increasing trend of IL-10 before day 13. After the pro-inflammatory stimulation with 2 ng mL<sup>-1</sup> TNF-  $\alpha$ , the IL-10 levels were suppressed and the IL-6 levels were raised significantly. (d) Comparison of cytokine secretion profiles of adipose-tissue-on-chip after adding different densities of J7 macrophages in the medium with (+Pio) or without (-Pio) pioglitazone. (e) Cytokine secretion profiles of the adipose-tissue-on-chip after pro-inflammatory LPS stimulation in the medium with (+Pio) or without (-Pio) pioglitazone. From (c)-(e), the results were measured from at least 3 samples under the same condition. Error bar: standard error.

stimulation with 2 ng mL<sup>-1</sup> of TNF-α, the adipocytes exhibited a significant change from anti-inflammatory into an inflammatory phenotype as evidenced by the elevated levels of IL-6 and suppressed expressions of IL-10, similar to the obesity-induced changes in the adipose tissue microenvironment. On day 15 after removing the TNF-α-conditioned medium, the adipocytes without the J7 macrophages continued expressing pro-inflammatory cytokines but nondetectable levels of anti-inflammatory cytokines (Fig. 4d), suggesting a low-grade inflammatory milieu in the adiposetissue-on-chip, confirming that we have successfully produced a biomimetic, obesity-induced, and inflammatory adipose tissue microenvironment. We then compared the cytokine secretion profiles of the adipose-tissue-on-chip after adding different densities of J7 macrophages. IL-6 and TNF- $\alpha$  levels have been observed to increase with the number of J7 macrophages introduced into the chip, indicating that the macrophages were mainly polarized into the inflammatory M1 phenotype, concurring with our previous immunofluorescence staining and analysis results (Fig. 3b) and other studies on obese adipose tissue macrophages. Juxtaposed with the observation of increasing CLS density (Fig. S4†), our results correlate CLS formation with the level of adipose tissue inflammation. The devices using medium without pioglitazone expressed higher levels of pro-inflammatory cytokines after D14, confirming the suppressive effect of pioglitazone on adipose tissue inflammation. These results suggest that CLS formation is cell and microenvironment-dependent and can be modulated under *in vitro* conditions to recapitulate aspects of adipose tissue inflammation in real time.

It has been well known that lipopolysaccharide (LPS) can initiate an acute pro-inflammatory response of macrophages and promote the secretion of pro-inflammatory cytokines TNF- $\alpha$  and IL-6. <sup>42</sup> Thus, to validate our sensing platform that can map phenotype changes as a response to inflammatory milieu alterations, we stimulated J7 macrophages with LPS (100 ng mL<sup>-1</sup>), both off-chip and on-chip, and subsequently quantified cytokine secretion profiles. First, we prestimulated J7 macrophages (density  $\sim 5 \times 10^4$  cells per mL) with 100 ng mL<sup>-1</sup> of LPS for 24 h in T75 flasks, then collected 50 μL of the supernatant samples from the J7 macrophage culture medium and loaded it into our microfluidic LSPR biosensor device for cytokine detection. We also collected the control samples from the J7 cell culture medium without LPS stimulation for comparison. Significant increases in TNF-α and IL-6 levels were observed in the supernatants collected

from LPS-stimulated J7 macrophages, consistent with previous studies (Fig. S5†).43,44

Then, we performed the on-chip LPS stimulation by simultaneously adding 100 ng mL<sup>-1</sup> of LPS and loading J7 macrophages into the adipose-tissue-on-chip cell culture chamber on day 14. The on-chip multiplexed cytokine secretion profiles were measured on day 15. Unlike the low-grade inflammation with IL-6 and TNF- $\alpha$  around 200-300 pg mL<sup>-1</sup> in the non-stimulated chips, LPS stimulation led to high-grade inflammation in the adipose-tissue-on-chip, displaying heightened secretion levels (>1500 pg mL<sup>-1</sup>) of IL-6. Interestingly, we also observed distinct IL-10 levels after LPS stimulation. This observation is consistent with those previously reported where the LPS challenge prompts the expression of antiinflammatory cytokines like IL-10 in multiple types of cells, such as 3T3L1 adipocytes,6 microglia,45 Kupffer cells,46 etc. Our integrated nanoplasmonic adipose-on-chip has proven to be a reliable platform to monitor dynamic multiplexed cytokine secretion profiles of cells in a biomimetic adipose tissue microenvironment.

#### Conclusion

Although many cytokine sensing techniques have been developed, they have been hindered by the complexity to troubleshoot signal acquisition, sensor integration, low sensitivity, or lack of multiplexity. Thus, this has stressed an urgent need to equip novel label-free cytokine biosensors to profile the dynamic in situ cytokine secretion behaviors of a complex biomimetic tissue microenvironment. In this work, we demonstrated a novel integration of a LSPR biosensor with a biomimetic microfluidic adipose-tissue-on-chip platform to quantitatively characterize the multiplexed cytokine secretion patterns of adipose tissue cells altered by pro-inflammatory stimulations. In particular, we were able to easily observe the appearance of the adipocytes and the on-chip formation of CLS in our microfluidic biomimetic adipose tissue microenvironment chip. With integrated antibody-conjugated AuNR LSPR barcode arrays, our platform enables simultaneous multiplexed measurements of pro-inflammatory (IL-6 and TNF-α) and antiinflammatory (IL-10 and IL-4) cytokines secreted by the adipocytes and macrophages. Our cytokine secretion assay was rapid (<30 min), sensitive ( $\sim20 \text{ pg mL}^{-1}$ ), and easy to implement for multiplexed and real-time detection. The multiplexed timecourse cytokine secretion data obtained from this work enabled us to monitor the dynamic, stage-specific responses of adipocytes and encircling macrophages during differentiation and pro-inflammatory stimulation in the adipose tissue microenvironment. To the best of our knowledge, this study is the first to integrate a label-free, multiplexed biosensor into a complex biomimetic tissue microenvironment and quantitatively characterize the dynamic cytokine secretion behaviors in a spatiotemporal manner. We envision this integrated 'adiposetissue-on-chip' biosensing platform will not only be applied as a precise drug-efficacy screening and prognostic tool for personalized treatment regimens and risk prevention against obesity but can also be adapted to other biomimetic microfluidic cultures to drive future research in precision immunology for personalized medicine.

#### Materials and methods

#### Microfluidic device fabrication

Poly-dimethylsiloxane (PDMS) was used to frame the microfluidic device to reconstruct a biomimetic adipose tissue microenvironment in vitro. Master molds were first fabricated on silicon substrates by employing photolithography with a SU-8 negative photoresist (2025, Microchem). The master molds were silanized with trichloro(1H,1H,2H,2H-perfluorooctyl)silane (448931, Sigma-Aldrich) vapor overnight under vacuum desiccation to facilitate subsequent release of PDMS from the molds. A PDMS precursor (Sylgard-184, Dow Corning) was prepared by mixing a PDMS curing agent with the base (wt:wt = 1:10), poured onto the molds, and cured overnight in a 60 °C oven. Two separate fully cured PDMS structures with microfluidic channels were fabricated using different molds: one for patterning the circulated AuNR biosensor barcodes on a glass substrate and the other for forming the on-chip culturing and cytokine detection layer (Fig. S1†).

#### Assembly of adipose-tissue-on-chip device and LSPR cytokine detection layer

To assemble the integrated culture and detection platform, we first permanently bound a clean 18 cm × 18 cm glass cover slide on the top side of the PDMS microfluidic device. The device was then sterilized by exposing it under UV light for 5 min. Subsequently, the device was inverted, producing a 4 mm diameter cylindrical chamber with a sealed bottom. The adipocytes and macrophages were then cultured on-chip in a single chamber in a cell culture incubator. Before taking each multiplexed cytokine measurement, a fresh glass substrate with a patterned AuNR sensing array was temporarily bound to the PDMS microfluidic device. The circular AuNR sensing array and microfluidic chamber were aligned under an optical microscope. After bonding, the whole device was then inverted to allow conditioned culture media to diffuse into the microchannels and AuNR sensing array for LSPR cytokine detection. After each measurement, the AuNRpatterned glass substrate was peeled off, and the device was put back into the incubator for on-chip cell culture.

#### Cell culture

Mouse 3T3L1 precursor adipocyte cell line (ATCC) and J774A.1 macrophages (ATCC) were cultured separately in the pre-adipocyte expansion medium containing 90% of Dulbecco's modified Eagle's medium (DMEM, sigma Al) supplemented with 10% bovine serum (Gibco) and 1% penicillin/streptomycin (Gibco) in T75 flasks. Both cell lines were grown in a 37 °C and 5% CO2 incubator to reach 80% confluence for any further experimentation.

Paper Lab on a Chip

#### On-chip adipocyte differentiation, maturation and inflammatory stimulation

The culture chamber was incubated in 1 mg mL<sup>-1</sup> fibronectin solution for 1 hour to help the adhesion of cells on the surface of glass. After removing fibronectin and washing, preadipocytes and 35 µL of cell culture medium were added into the chamber for the on-chip culture experiment. After the 3T3L1 pre-adipocytes were loaded into the adipocyte culture chamber (1000 cells per device) and cultured for 2 days, the pre-adipocyte expansion medium was replaced with differentiation medium to initiate adipocyte differentiation, and we denoted the date as day 0. The differentiation medium contains 90% DMEM (Caisson), 10% FBS (Gibco), 1% penicillin/ streptomycin (Gibco), 1.0 μg mL<sup>-1</sup> insulin (Gibco), 1.0 μM dexamethasone, and 0.5 mM methylisobutylxanthine (IBMX) to chemically induce the differentiation of the 3T3L1 cells. To enhance adipocyte differentiation, the differentiation medium was replaced with a pioglitazone (0.2 µM; Alfa Aesar)supplemented adipocyte maintenance medium on day 2. The adipocyte maintenance medium contains 90% DMEM (Caisson), 10% FBS (Gibco), 1% penicillin/streptomycin (Gibco), and 1.0 µg mL<sup>-1</sup> insulin (Gibco). The adipocytes were then continuously cultured in the adipocyte maintenance medium with pioglitazone for another 11 days with the culture medium replaced every 2-3 days. On day 13, 2 ng mL<sup>-1</sup> of TNF-α (eBioscience) was added into the adipocyte maintenance medium, stimulating the inflammatory microenvironment for 24 hours. On day 14, the medium with TNF-α was replaced by a normal adipocyte maintenance medium with 0.2 µM pioglitazone. Different amounts of J7 macrophages (0, 500, and 1000 cells, denoted as 0× Mac, 1× Mac and 2× Mac) were simultaneously introduced into three different devices to mimic different levels of inflammation. The 3T3L1 adipocytes and J7 macrophages were co-cultured in the devices for another 24 hours before taking cytokine measurement at the final stage. A control experiment following the same procedure but without the addition of pioglitazone was performed and compared. All the cells were incubated at 37 °C with 5% CO<sub>2</sub> and 100% humidity in a CO2 cell culture incubator.

#### LSPR nanoplasmonic biosensor microarray fabrication

The fabrication of LSPR nanoplasmonic biosensor microarray is shown as a schematic in Fig. S2.† A piranha-cleaned glass substrate was first oxygen-plasma treated at 20 W for 120 s. Then, a colloidal solution suspending positively charged CTAB-coated AuNRs (Nanoseedz, Hong Kong) was flowed into the PDMS microfluidic patterning channels (Fig. S1d†) covered by the plasma-treated glass substrate. The surface of the glass substrate was negatively charged. The AuNRs were immobilized onto the glass substrate by means of electrostatic interactions and parallel sensor array patterns were formed. Subsequently, 1 mM 11-mercaptoundecanoic acid (Sigma-Aldrich) was dissolved in 10% ethanol, loaded into the microfluidic patterning channels, and incubated overnight to functionalize the AuNR surfaces with the thiol

anchor group, which replaced CTAB through a ligand exchange process. 0.4 M EDC (1-ethyl-3-[3-(dimethylamino)propyl]carbodiimide hydrochloride, Thermo Scientific) and 0.6 M NHS (N-hydroxysuccinimide, Thermo Scientific) were mixed at a 1:1 volume ratio in 0.1 M MES (2-(4-morpholino) ethanesulfonic acid, Thermo Scientific) solution. The EDC/ NHS/MES solution was loaded into the same microfluidic channels and incubated for 30 min to activate the ligand. This was followed by antibody coating of the AuNR sensor patterns that involved loading of probe antibodies (antimouse IL-4, IL-6, IL-10, and TNF-α; eBioscience, USA) in PBS solution at a concentration of 50 μg mL<sup>-1</sup> into individual patterning channels. Subsequently, 3% BSA in deionized water solution was loaded into the channels and incubated for 20 min for sensor surface passivation to eliminate nonspecific binding of biomolecules. At the end of every incubation step above, the sensor surfaces were thoroughly washed using deionized water, and any excessive solution and unbound molecules were removed.

#### LSPR dark-field imaging for cytokine detection

Before each multiplexed cytokine measurement, a freshly made glass substrate with the AuNR LSPR biosensor microarray chip was temporarily bonded onto the side of the culture chamber with the microchannel patterns. The alignment of the circular AuNR arrays and the microchannels were operated using an optical microscope. The device was then reversed to have the cell culture medium diffuse into the microchannels during the LSPR measurement. After the measurement, the AuNR-patterned glass substrate was peeled off, and the device was sent back to the incubator to continue the on-chip cell culture. The LSPR biosensor microarray chip was mounted on the motorized stage of an upright microscope (Axio Imager 2, Zeiss) to position the on-chip sensing spot at ease and to automate the signal scanning. A darkfield condenser (NA = 1.45) was closely placed to the backside of the glass substrate (the opposite side of the AuNRdeposited sensor side) using lens oil. The light scattered from the AuNR nanoplasmonic biosensor arrays was collected using a 10× objective lens under the chip and then filtered using a band-pass filter (674-686 nm, Semrock). This light signal was collected using an electron multiplying CCD (EMCCD, Photometrics) camera (Fig. S3†). The captured LSPR images were then processed using a customized MATLAB program to selectively detect the intensity changes of the LSPR images in a microfluidic channel resulting from the cytokine surface binding to AuNRs. Image analysis was performed using our customized MATLAB code.

#### Spectral shift measurement of biomolecule binding using a spectrophotometer

The scattering spectrum of the AuNRs during each step of biomolecule binding was measured using a fiber spectrometer (Ocean Optics, UR2000). The spectrometer was mounted onto the camera C-mount port of the dark-field upright

microscope (Axio Imager 2, Zeiss) to check the dark-field scattering spectrum of the AuNR substrate. The spectral shift at each bio-conjugation step was monitored (Fig. S3†).

#### Cytokine measurement with ELISA immunoassays

The validation of cytokine measurement was carried out by measuring PBS solutions spiked with different concentrations of cytokines (mouse IL-4, IL-6, IL-10, and TNF-α; eBioscience, USA) using both LSPR microarrays and the gold-standard ELISA. ELISA kits (Mouse IL-4 ELISA MAX<sup>TM</sup> Deluxe, Mouse IL-6 ELISA MAX<sup>TM</sup> Deluxe, Mouse IL-10 ELISA MAX<sup>TM</sup> Deluxe, and Mouse TNF-α ELISA MAXTM Deluxe, Biolegend) were used in this study according to manufacturer's protocols. Briefly, cytokine solutions or cell culture supernatants were collected as samples. Capture antibody solution was added into all the wells of a 96-well plate provided in the kit, and the plate was subsequently sealed and incubated at 4 °C overnight. After washing and blocking, 100 µL of each standards and samples were added into the wells and were incubated for 2 hours at room temperature. The wells were then incubated with detection antibody for 1 hour, followed by washing and incubation with HRP-labeled Avidin for 30 minutes. The TMB mixture (1:1) was then applied to visualize chemiluminescence for 20 minutes in the dark. Then, 100 µL of 2 N sulfuric acid solution was added in each well to stop the reaction. The reading of ELISA results was carried out using a plate reader (SpectraMax i3, Molecular Devices) by reading the absorbance at 450 nm within 15 min after adding the stop solution.

#### Immunofluorescence staining and analysis

We fixed and stained the cells cultured on the chip after day 15. The cells were fixed with 4% paraformaldehyde (15711, Electron Microscopy Sciences) for 30 min, permeabilized with 0.3% Triton X- 100 (11332481001, Sigma-Aldrich) for 10 min, and then blocked with 3% bovine serum for 1 h on ice to eliminate nonspecific binding. Specifically, we stained M1 phenotype macrophages by incubating the chip with iNOS primary antibodies (NB300605, Novus Biologicals, 5 μg mL<sup>-1</sup>) for 1 h, and then visualized with Alexa Fluor 555 conjugated goat anti-mouse IgG secondary antibodies (Invitrogen, 5 mg mL<sup>-1</sup>). All the cell nuclei were stained with DAPI. The fluorescence images were obtained using an inverted microscope (Zeiss Axio Observer.Z1) equipped with a digital CMOS camera (ORCA-Flash4.0 LT digital CMOS camera, Hamamatsu Photonics) and a 10× objective lens.

#### Conflicts of interest

There are no conflicts of interest to declare.

#### Acknowledgements

We acknowledge financial supports from the National Science Foundation (CBET 1701322 to W. C. and CBET 1701363 to P. C.), the National Institute of Health (NIH/NIBIB 1R21EB025406-

01A1 to W. C.), the New York University Global Seed Grant, and NYU Clinical and Translational Science Institute Collaborative Translational Pilot Award (NIH/NCATS 1UL1 TR001445). J. O. A. was supported by the Sackler Foundation and the Helmsley Center for Disorders of the Digestive System, both at Rockefeller University, during the initial phases of this work.

#### References

- 1 E. Dalmas, K. Clément and M. Guerre-Millo, *Trends Immunol.*, 2011, 32, 307–314.
- 2 M. Zeyda and T. M. Stulnig, *Immunol. Lett.*, 2007, 112, 61-67.
- 3 P. G. Morris, C. A. Hudis, D. Giri, M. Morrow, D. J. Falcone, X. K. Zhou, B. Du, E. Brogi, C. B. Crawford, L. Kopelovich, K. Subbaramaiah and A. J. Dannenberg, *Cancer Prev. Res.*, 2011, 4, 1021–1029.
- 4 S. Cinti, G. Mitchell, G. Barbatelli, I. Murano, E. Ceresi, E. Faloia, S. Wang, M. Fortier, A. S. Greenberg and M. S. Obin, *J. Lipid Res.*, 2005, 46, 2347–2355.
- 5 A. S. Haka, V. C. Barbosa-Lorenzi, H. J. Lee, D. J. Falcone, C. A. Hudis, A. J. Dannenberg and F. R. Maxfield, *J. Lipid Res.*, 2016, 57, 980–992.
- 6 F. S. Lira, J. C. Rosa, C. A. Cunha, E. B. Ribeiro, C. Oller do Nascimento, L. M. Oyama and J. F. Mota, *Lipids Health Dis.*, 2011, 10, 37.
- 7 Z. Frankenstein, U. Alon and I. R. Cohen, *Biol. Direct*, 2006, 1, 32.
- 8 G. Liu, M. Qi, M. R. Hutchinson, G. Yang and E. M. Goldys, *Biosens. Bioelectron.*, 2016, 79, 810–821.
- 9 T. Schenk, H. Irth, G. Marko-Varga, L.-E. Edholm, U. Tjaden and J. van der Greef, *J. Pharm. Biomed. Anal.*, 2001, 26, 975–985.
- 10 P. Chen, N.-T. Huang, M.-T. Chung, T. T. Cornell and K. Kurabayashi, *Adv. Drug Delivery Rev.*, 2015, 95, 90–103.
- 11 R. van den Hurk and S. Evoy, *Sens. Actuators*, *B*, 2013, 176, 960-965.
- 12 P. Dutta, J. Sanseverino, P. G. Datskos and M. J. Sepaniak, *NanoBiotechnology*, 2005, 1, 237–244.
- 13 T.-S. Pui, A. Agarwal, F. Ye, Y. Huang and P. Chen, *Biosens. Bioelectron.*, 2011, 26, 2746–2750.
- 14 Y. Liu, N. Tuleouva, E. Ramanculov and A. Revzin, *Anal. Chem.*, 2010, **82**, 8131–8136.
- 15 T. S. Pui, P. Kongsuphol, S. K. Arya and T. Bansal, *Sens. Actuators, B*, 2013, **181**, 494–500.
- 16 P. Kongsuphol, H. H. Ng, J. P. Pursey, S. K. Arya, C. C. Wong, E. Stulz and M. K. Park, *Biosens. Bioelectron.*, 2014, 61, 274–279.
- 17 M. S. Luchansky and R. C. Bailey, *J. Am. Chem. Soc.*, 2011, 133, 20500–20506.
- 18 S. Mandal, J. M. Goddard and D. Erickson, *Lab Chip*, 2009, 9, 2924.
- 19 M. S. Luchansky and R. C. Bailey, *Anal. Chem.*, 2010, 82, 1975–1981.
- 20 F. Inci, C. Filippini, M. Baday, M. O. Ozen, S. Calamak, N. G. Durmus, S. Wang, E. Hanhauser, K. S. Hobbs, F. Juillard, P. P. Kuang, M. L. Vetter, M. Carocci, H. S. Yamamoto, Y.

- Takagi, U. H. Yildiz, D. Akin, D. R. Wesemann, A. Singhal, P. L. Yang, M. L. Nibert, R. N. Fichorova, D. T.-Y. Lau, T. J. Henrich, K. M. Kaye, S. C. Schachter, D. R. Kuritzkes, L. M. Steinmetz, S. S. Gambhir, R. W. Davis and U. Demirci, Proc. Natl. Acad. Sci. U. S. A., 2015, 112, E4354-E4363.
- 21 Y.-C. Huang, C.-Y. Chiang, C.-H. Li, T.-C. Chang, C.-S. Chiang, L.-K. Chau, K.-W. Huang, C.-W. Wu, S.-C. Wang and S.-R. Lyu, Analyst, 2013, 138, 4599.
- 22 T. Huang, P. D. Nallathamby and X.-H. N. Xu, J. Am. Chem. Soc., 2008, 130, 17095-17105.
- 23 C.-Y. Chiang, M.-L. Hsieh, K.-W. Huang, L.-K. Chau, C.-M. Chang and S.-R. Lyu, *Biosens. Bioelectron.*, 2010, 26, 1036–1042.
- 24 J. Martinez-Perdiguero, A. Retolaza, L. Bujanda and S. Merino, Talanta, 2014, 119, 492-497.
- 25 S. R. Corrie and M. Plebanski, Mol. Immunol., 2018, 98, 28-35.
- 26 M. S. Luchansky and R. C. Bailey, J. Am. Chem. Soc., 2011, 133, 20500-20506.
- 27 B. R. Oh, P. Chen, R. Nidetz, W. McHugh, J. Fu, T. P. Shanley, T. T. Cornell and K. Kurabayashi, ACS Sens., 2016, 1, 941-948.
- 28 B.-R. Oh, N.-T. Huang, W. Chen, J. H. Seo, P. Chen, T. T. Cornell, T. P. Shanley, J. Fu and K. Kurabayashi, ACS Nano, 2014, 8, 2667-2676.
- 29 S. Wang, S. Ota, B. Guo, J. Ryu, C. Rhodes, Y. Xiong, S. Kalim, L. Zeng, Y. Chen, M. A. Teitell and X. Zhang, Nano Lett., 2011, 11, 3431-3434.
- 30 X. Li, M. Soler, C. I. Özdemir, A. Belushkin, F. Yesilköy and H. Altug, Lab Chip, 2017, 17, 2208-2217.
- 31 W. Chen, N.-T. Huang, B. Oh, R. H. W. Lam, R. Fan, T. T. Cornell, T. P. Shanley, K. Kurabayashi and J. Fu, Adv. Healthcare Mater., 2013, 2, 965-975.
- 32 N.-T. Huang, W. Chen, B.-R. Oh, T. T. Cornell, T. P. Shanley, J. Fu and K. Kurabayashi, Lab Chip, 2012, 12, 4093.
- 33 Y. Song, P. Chen, M. T. Chung, R. Nidetz, Y. Park, Z. Liu, W. McHugh, T. T. Cornell, J. Fu and K. Kurabayashi, Nano Lett., 2017, 17, 2374-2380.

- 34 Y. B. Zheng, B. Kiraly, P. S. Weiss and T. J. Huang, Nanomedicine, 2012, 7, 751-770.
- 35 P. Chen, M. T. Chung, W. McHugh, R. Nidetz, Y. Li, J. Fu, T. T. Cornell, T. P. Shanley and K. Kurabayashi, ACS Nano, 2015, 9, 4173-4181.
- 36 J. M. Wentworth, G. Naselli, W. A. Brown, L. Doyle, B. Phipson, G. K. Smyth, M. Wabitsch, P. E. O'Brien and L. C. Harrison, Diabetes, 2010, 59, 1648-1656.
- 37 A. J. Haes, C. L. Haynes, A. D. McFarland, G. C. Schatz, R. P. Van Duyne and S. Zou, MRS Bull., 2005, 30, 368-375.
- 38 C. Church, M. Horowitz and M. Rodeheffer, Adipocyte, 2012, 1, 38-45.
- 39 X. Cui, R.-T. T. Morales, W. Qian, H. Wang, J.-P. Gagner, I. Dolgalev, D. Placantonakis, D. Zagzag, L. Cimmino, M. Snuderl, R. H. W. Lam and W. Chen, Biomaterials, 2018, 161, 164-178.
- 40 C. N. Lumeng, J. L. Bodzin and A. R. Saltiel, J. Clin. Invest., 2007, 117, 175-184.
- 41 P. A. Permana, W. Zhang, M. Wabitsch, P. Fischer-Posovszky, W. C. Duckworth and P. D. Reaven, Am. J. Physiol., 2009, 296, E1076-E1084.
- 42 G. Yücel, Z. Zhao, I. El-Battrawy, H. Lan, S. Lang, X. Li, F. Buljubasic, W.-H. Zimmermann, L. Cyganek, J. Utikal, U. Ravens, T. Wieland, M. Borggrefe, X.-B. Zhou and I. Akin, Sci. Rep., 2017, 7, 2935.
- 43 V. Seow, J. Lim, A. Iyer, J. Y. Suen, J. K. Ariffin, D. M. Hohenhaus, M. J. Sweet and D. P. Fairlie, J. Immunol., 2013, 191, 4308-4316.
- 44 X. Cui, R.-T. T. Morales, W. Qian, H. Wang, J.-P. Gagner, I. Dolgalev, D. Placantonakis, D. Zagzag, L. Cimmino, M. Snuderl, R. H. W. Lam and W. Chen, Biomaterials, 2018, 161, 164-178.
- 45 C. J. Henry, Y. Huang, A. M. Wynne and J. P. Godbout, Brain, Behav., Immun., 2009, 23, 309-317.
- 46 P. Knoll, J. Schlaak, A. Uhrig, P. Kempf, K.-H. M. zum Büschenfelde and G. Gerken, J. Hepatol., 1995, 22, 226-229.